Oral Microbial Extracellular DNA as an Initiator of Periodontitis through Gingival Degradation by Fibroblast-derived Cathepsin K

Takeru Kondo
UCLA School of Dentistry
Hiroko Okawa
UCLA School of Dentistry
Akishige Hokugo
Geffen School of Medicine at UCLA
Bhumika Shokeen
UCLA School of Dentistry
Oskar Sundberg
University of Southern California
Yiying Zheng
University of Southern California
Charles McKenna
University of Southern California https://orcid.org/0000-0002-3540-6663
Renate Lux
UCLA School of Dentistry https://orcid.org/0000-0003-3253-0471
Ichiro Nishimura (inishimura@dentistry.ucla.edu)
UCLA School of Dentistry https://orcid.org/0000-0002-3749-9445

Article

Keywords:

Posted Date: April 20th, 2022

DOI: https://doi.org/10.21203/rs.3.rs-1341027/v1

Version of Record: A version of this preprint was published at Communications Biology on September 14th, 2022. See the published version at https://doi.org/10.1038/s42003-022-03896-7.

Abstract

Periodontitis is a highly prevalent disease leading to uncontrolled osteoclastic jawbone resorption and ultimately to edentulism. While the interaction between dysbiotic biofilm communities and host oral barrier immunity has been extensively studied, much less is known about the disease onset mechanism. We report here its initial pathological mechanism revealed by a new in vivo molecular imaging platform using a highly sensitive, Osteoadsorptive Fluogenic Sentinel (OFS) probe that emits a fluorescent signal triggered by cathepsin K (Ctsk) activity. Unexpectedly, a strong OFS signal was already observed before the establishment of chronic inflammation and bone resorption in a ligature-induced mouse model of periodontitis. Single cell RNA sequencing revealed that the cellular source of early Ctsk was not osteoclasts but gingival fibroblasts. Furthermore, the in vivo OFS signal was activated when Toll-Like Receptor 9 (TLR9) ligand or oral biofilm extracellular DNA (eDNA) was topically applied to the mouse palatal gingiva. By contrast, TLR2/4 ligand and planktonic oral microbial mixture failed to activate the in vivo OFS signal. This previously unrecognized interaction between oral microbial eDNA and gingival Ctsk provides a pathological mechanism for disease initiation and a new strategic basis for early diagnosis and intervention of periodontitis.

Introduction

Periodontal disease is a highly prevalent non-communicable inflammatory disease of the tooth-supporting tissues that affects nearly 70% of adults over 65 years old in the U.S. [1], and significantly contributes to the global health burden [2]. The pivotal devastation of periodontitis is uncontrolled tooth-supporting jawbone resorption by overly activated osteoclasts, which is strongly correlated with dental morbidity [3]. It has been postulated that dysbiotic shifts of oral commensal bacterial communities cause aberrant oral barrier immunity [4], including local differentiation of Th17 cells [5] and mobilization of neutrophils [6]. These clusters of highly potent immune cells not only develop and sustain chronic inflammation in the oral barrier tissue but also stimulate localized osteoclastogenesis. The clinical diagnosis of periodontitis is currently based, in large part, on dental radiographs of the alveolar bone morphological changes [7]. However, when bone resorption is clearly detected radiographically, the disease has already progressed and irreversible changes to the bone level, which often lead to tooth loss, have manifested.

The degree of periodontal pocket formation generated by the loss of gingival attachment to the affected dentition also serves as a critical diagnostic measure for the severity of periodontitis [8]. The periodontal pocket provides an anaerobic environment suitable for colonization with periodontal pathogens that can trigger dysbiotic shifts of oral commensal microbial communities. The periodontal pocket is formed by the disarrangement and degradation of gingival and periodontal ligament extracellular matrix (ECM) and the apical extension of the junctional epithelium [9]. Initial gingival inflammatory responses are prompted by the presence of oral biofilm communities at the tooth-tissue interface of the gingival sulcus [10]. A study of human cadaver tissues revealed that periodontal pocket formation was accompanied by degradative

changes in gingival and periodontal ligament fibroblasts and collagenous ECM [11]. However, a knowledge gap still exists: how gingival and periodontal ligament ECM is degraded prior to the development of chronic oral barrier inflammation; and how oral microorganisms contribute to the initiation of periodontal pocket development.

Osteoclasts secrete cathepsin K (Ctsk), a cysteine protease that degrades the bone collagen matrix [12]. Ctsk was also found secreted by other cell types that contributed to pathological processes of tendon [13] and vascular tissues [14]. We have recently developed a bone-targeting, Ctsk-activated fluorescent sensor, Osteoadsorptive Fluorogenic Sentinel (OFS) probes, in which a bisphosphonate (BP) moiety is covalently attached to a fluorophore linked via a Ctsk octapeptide substrate to an internal quencher that suppresses external fluorescence by Förster resonance energy transfer (FRET). The inclusion of the BP modifier results in stabilization of OFS probe to bone surfaces, where an external fluorescent signal is activated if locally released Ctsk cleaves the linker [15]. The sensitivity of OFS fluorescence activation has been demonstrated at in a humanized mouse model of multiple myeloma that the OFS signal was detected at the orthotropic grafted site of luciferase-tagged multiple myeloma cell prior to the detection of luciferase activity [15].

In this investigation, we employed OFS probes in a murine experimentally induced periodontitis model to elucidate the pathological mechanism of periodontitis initiation by detecting the early Ctsk activity prior to the manifestation of radiographic bone changes. This new *in vivo* research platform surprisingly identified the early Ctsk activity of gingival fibroblasts immediately after the ligature placement. Furthermore, the *in vivo* OFS signal was detected when microbial extracellular DNA (eDNA) was topically applied to mouse palatal gingiva. This previously unrecognized relationship between eDNA and gingival Ctsk provides novel evidence for the processes involved in the initial progression of periodontitis leading to new diagnostic and therapeutic modalities.

Results

Ctsk activation prior to inflammation and bone resorption in a ligature-induced mouse periodontitis model

We used the ligature-induced mouse periodontitis model (**Figure S1a**), which was previously reported to establish chronic inflammation and alveolar bone resorption 5 to 7 days after silk suture placement around the maxillary second molar [5, 16]. Following gingival swelling (**Figure S1b**) and induction of inflammatory cytokine gene expression (**Figure S1c**), clear radiographic alveolar bone reduction was observed on Day 7 (**Figure 1a** and **1b**). To monitor disease initiation and progression, we determined Ctsk activity using the OFS probe (**Figure 1c** and **1d**) [15]. We synthesized a fluorescein-OFS probe (OFS-1) with a 5-FAM fluorophore which emits at 518 nm, quenched by BHQ-1, and a far-red OFS probe (OFS-3) which emits at 650 nm (SulfoCy5 quenched by BBQ-650) (**Figure 1d** and **S2**). Both OFS-1 and OFS-3 gave rise to similar results. Unlike a commercially available Ctsk FRET probe without bone retention properties, the incorporation of a bone anchoring property into the OFS probe allowed localization to the jawbone surface, which provided sensitive detection of local Ctsk activity (**Figure 1e**).

The OFS probe administration by intravenous (IV) injection was combined with the ligature-induced periodontitis mouse model. This new *in vivo* research platform clearly demonstrated that Ctsk was activated from Day 1 after ligature placement (**Figure 1f**). These results suggest that Ctsk activation occurred in the very early stages of periodontitis development prior to the establishment of chronic gingival inflammation and alveolar bone resorption.

Ctsk induced periodontal connective tissue degradation

Immunohistochemical (IHC) staining revealed the presence of Ctsk in the periodontal ligament and gingival connective tissue on Day 1 (**Figure 2a**). On Day 7, the Ctsk IHC staining in the gingival connective tissue remained in the area beneath the epithelial layer, and Ctsk was also strongly observed in osteoclasts on the surface of alveolar bone (**Figure 2a**). Detachment of the junctional epithelium from the tooth and degradation of collagen in the connective tissue were observed following the appearance of Ctsk in the periodontal ligament and gingival connective tissue. These results indicated that Ctsk was secreted by cells in the periodontal ligament and gingiva other than osteoclasts and contributed to the degradation of the connective tissue extracellular matrix (ECM).

To explore the pathological function of Ctsk in periodontitis, odanacatib, an inhibitor of Ctsk [17], was administered to mice upon ligature placement. Picrosirius red staining showed that ligature placement induced severe degradation of gingival connective tissue and periodontal ligament on Day 7, whereas it was significantly attenuated by the oral gavage administration of odanacatib (**Figure 2b** and **2c**). Moreover, bone resorption was also suppressed by odanacatib (**Figure 2d** and **2e**) as expected [18]. These results suggest that Ctsk could play important roles in the early stages of periodontal tissue degradation and attachment loss as well as osteoclastic alveolar bone resorption.

Identification of the cellular source of Ctsk in the early periodontitis lesion

To identify the cellular source of Ctsk in the gingival tissue at Day 1 of ligature placement, we performed single cell RNA-sequencing (scRNA-seq). The ligature side of the palatal gingiva at 1 day after ligature placement was harvested and exposed to two types of enzymes (**Figure 2f** and **2g**). We identified five major cell types dissociated from the palatal gingiva by cluster mapping using the expression of lineage specific genes (**Figure 2h** and **S3**). scRNA-seq data were screened for *Ctsk* and a high level of *Ctsk* expression was observed in the fibroblast cluster. Our data indicated that gingival fibroblasts were the major cellular source of Ctsk in the initial stage of periodontitis development (**Figure 2i**).

TLR9 stimulation induced Ctsk activation and gingival swelling

Periodontitis is initiated by microbial biofilms that accumulate in the gingival crevice, and these biofilms are formed by microorganisms that are embedded in a self-produced matrix of extracellular polymeric substances (EPS) [19]. In the present study, cultured human oral microbial biofilm or planktonic bacteria were topically applied to the mouse palatal gingiva covered by a custom-made oral appliance for 1 hr. Three days after the topical application of human oral microbial biofilm or planktonic bacteria, OFS was

administered by intravenous injection, and the resulting OFS fluorescence was measured the following day. Examination of OFS activation revealed that human oral microbial biofilm activated the OFS signal, while the OFS activation was not detected in the corresponding planktonic bacteria topical application group (**Figure 3a** and **3b**). From these results, we hypothesized that components of the EPS matrix played a role in gingival Ctsk activation.

Toll-like receptors (TLRs) are known to play critical roles in the defense against microorganisms and to induce inflammatory responses [20]. Microbial infections are recognized by TLRs via pathogen-associated molecular patterns such as di/triacylated lipopeptides (TLR1/2) [21], lipopolysaccharide (LPS) (TLR2/4) [22] and unmethylated microbial CpG DNA sequences (TLR9) [23]. This study evaluated the role of TLR2/4 and TLR9 in the activation of gingival Ctsk. To this end, LPS from *Porphyromonas gingivalis* and synthetic unmethylated CpG oligonucleaotide (CpG ODN), respectively, were topically applied to the mouse palate for 1 hr, followed by examination of OFS activation on Day 4. The TLR9 ligand CpG ODN activated the OFS signal significantly more than the TLR2/4 ligand LPS (**Figure 3c** and **3d**). IHC analysis showed that CpG ODN activated Ctsk in gingival fibroblasts localized below the epithelial layer (**Figure 3e**). Moreover, Ctsk positive gingival fibroblasts were found within the disintegrated gingival connective tissue area, similar to the observation in ligature-induced periodontitis (**Figure 2a**).

The expression of proinflammatory cytokine genes such as *IL-6* and *IL-17A* was increased by CpG ODN using real time RT-PCR (**Figure 3f**). We separately compared gene expression patterns related to initiation of periodontitis in the gingival samples that were subjected to application of CpG ODN or LPS using scRNA-seq. CpG ODN induced higher expression of *IL-1β, IL-6, TNF* and *M-CSF* in myeloid cells compared to LPS, while similar *TGF-β1* expression between the CpG ODN and LPS groups was observed in B cells, T cells and myeloid cells (**Figure 3g**).

Mechanism of gingival fibroblast Ctsk activation by CpG ODN

TLR9 is predominantly located intracellularly in immune cells including dendritic cells that are known to function as antigen presenting cells in the oral barrier tissue [24]. In a psoriasis mouse model, drug induced Ctsk inhibition reduced the inflammatory reaction mediated by the downregulation of cytokine expression in dendritic cells [25]. Therefore, we initially expected gingival epithelial dendritic cells (Langerhans cells) or oral barrier dendritic cells to be the primary sensor of CpG ODN. Analysis of scRNA-seq data suggested the presence of *Langerin*+ cells in the myeloid cell cluster of Day 1 gingiva (**Figure 4a**) as well as untreated control gingiva (**Figure S4a**). The myeloid cell cluster was further subclustered and one subcluster was found to express *Langerin, Epcam* and *CD11c* (**Figure 4b** and **S4b**) indicating that Langerhans cells dissociated from gingival epithelium were included in the myeloid cell cluster.

The scRNA-seq data of the myeloid cell subclusters were further examined for TLR gene expression (**Figure 4c** and **S4c**) but TLR2/4 or TLR9 were not detected in the Langerhans cells. As activation and stability of TLRs is not only regulated by the putative gene transcription but also by the post-translational modifications such as proteolytic cleavage and phosphorylation [26], we investigated the gene expression

of the downstream signal transduction cascades initiated by activated TLR9. We found that the downstream genes *MyD88*, *Irak1*, *Tak1* and *Nf-kb* were highly expressed in the fibroblast cluster in our scRNA-seq analysis (**Figure 4d**). We thus hypothesized that gingival fibroblasts might possess the TLR9 sensing mechanism. RT qPCR of primary gingival fibroblasts harvested from untreated control mice showed a high steady state level of *TLR9* mRNA (**Figure 4e**). To validate the TLR9 function in relation to Ctsk, gingival fibroblasts were cultured in the presence of serially diluted CpG ODN. ELISA of the culture supernatant and the fibroblast homogenate revealed elevated Ctsk levels (**Figure 4f** and **4g**, respectively). Ctsk induction within gingival fibroblasts showed a dose dependent increase with the peak at 1 μM CpG ODN supplementation. By contrast, the Ctsk secretion to the culture supernatant indicated a more sensitive response peaking at 0.1 μM CpG ODN supplementation. The data also indicated that possibly different mechanisms were involved in the TLR9-activated secretion and accumulation of Ctsk in gingival fibroblasts.

Oral microbial eDNA may play a role in the initiation of periodontitis

We demonstrated that oral microbial biofilm and unmethylated CpG ODN activated the OFS signal *in vivo* at significantly higher levels compared to planktonic bacteria (**Figure 3a** and **3b**) or LPS (**Figure 3c** and **3d**). Microbial DNA is less methylated at its CpG sequences than mammalian genes and thus triggers TLR9 more effectively. To investigate if human oral microbial DNA was a ligand for TLR9, we separately isolated microbial extracellular cellular DNA (eDNA) and intracellular genomic DNA (iDNA) from oral microbial biofilms. Microbial eDNA is a pivotal structural component of microbial biofilms [27] that can be in contact with gingival tissue. Topical application of both eDNA and iDNA to the mouse palatal gingiva indeed activated Ctsk (**Figure 5a**); however, the effect of eDNA was stronger compared to the same amount of iDNA (**Figure 5b**).

We then investigated if eDNA was produced in the ligature-induced mouse periodontitis model. Palatal gingival swabs were obtained before (D0), 1 day (D1) and 7 days (D7) after ligature placement. The mouse oral microbial samples harvested from the swabs was evaluated by 16S rRNA sequencing. The oral swab microbial composition at the genus level appeared to be modulated after the ligature placement, in which *Enterococcus* was notably increased (**Figure 5c**) consistent with a previously published report [5]. However, eDNA was not isolated from the gingival swab samples. By contrast, the ligatures recovered at D1 and D7 were successfully used to harvest eDNA and iDNA. Oral microbial composition analysis from 16S rRNA sequencing revealed that the biofilm community associated with the ligature was different from the untreated mouse palatal gingival swab samples (D0); however, showed some resemblance to the palatal gingival swab samples after the ligature placement. The ligature-associated microbial community composition (iDNA) appeared to be less diverse than the corresponding eDNA (**Figure 5c**).

SYTOX Green-staining disclosed an eDNA meshwork spreading throughout the EPS of subgingival plaque samples collected from human subjects with diagnosed periodontitis (**Figure 5d**). The recovered ligatures from the mouse periodontitis model similarly contained SYTOX Orange-stained eDNA-like

structure (**Figure 5d**). These data validated the presence of eDNA in human oral biofilms and mouse ligatures recovered from the periodontitis model.

Discussion

The present study used a new bone-targeting OFS FRET-based detection system of Ctsk activity *in vivo* and directly implicates fibroblastic Ctsk induced by oral microbial eDNA in the genesis of gingival tissue degradation due to periodontitis. The physiological and pathological function of Ctsk has been investigated by well-established research platforms such as immunohistochemistry, *in situ* hybridization, knockout mutant mice, and chemical inhibitors. Ctsk is a lysosomal cysteine protease with strong collagenolytic activity known to mediate bone resorption by osteoclasts [28]. Ctsk in the gingival crevicular fluid of periodontitis patients was elevated compared to healthy patients, which was thought to reflect increased osteoclastic activity in periodontal tissues [29, 30]. A role of Ctsk in the periodontal bone resorption has been demonstrated using Ctsk knockout mice [31] and Ctsk inhibitor [18]. Thus, it has been believed that osteoclast-derived Ctsk plays the predominant role in the periodontal degradation and periodontitis development. The present study applied the OFS probe in a periodontitis mouse model and demonstrated the Ctsk activity in the context of the time course pathological development (**Figure 1**). The unique observation was the clear detection of Ctsk activity in the periodontal tissue prior to the establishment of chronic inflammation and osteoclast induction.

Recently, the cellular source of Ctsk other than osteoclasts has been reported. An immunohistochemical study of the human periodontitis gingival tissue reported the presence of Ctsk in macrophage-like cells, fibroblast-like cells, vascular endothelial cells, and gingival epithelial cells [32]; however, the key cellular source of the degrading protease was left unclear. The present study applied a high-definition transcriptome analysis using scRNA-seq and identified gingival fibroblasts as the early and predominant cellular source of *Ctsk* (**Figure 2i**). Our study demonstrates that Ctsk from gingival fibroblasts is directly implicated in the initial gingival and periodontal ligament connective tissue degradation (**Figure 2a-2c**) leading to the periodontal pocket formation harboring a pathological environment.

It is well established that periodontitis is caused by oral microbial stimuli in the periodontal pocket; however, unlike many other infectious diseases, the etiology is polymicrobial instead of involving individual pathogens. Oral biofilms are composed of heterogeneous, polymicrobial communities encased in a matrix of EPS, which can be recognized by the host via pattern recognition receptors such as the TLRs. Further using the new *in vivo* research platform, we demonstrated that human oral biofilm, not planktonic bacteria, led to the induction of Ctsk activation and inflammation (**Figure 3a**). The EPS matrix is composed of polysaccharides, lipids, proteins and eDNA [33]. The LPS of *P. gingivalis* has been considered as a prominent factor in the induction of an inflammatory host response through TLR2/4, resulting in periodontitis [34]. On the other hand, TLR9 signaling has emerged as a potential trigger of inflammation in periodontitis. The expression levels of inflammatory and osteoclastogenic cytokines were significantly elevated in the gingival tissue of WT mice inoculated with *P. gingivalis* but not in the

corresponding *TLR9* knockout mice [35]. Our study shows that the TLR9 ligand unmethylated CpG ODN induced not only Ctsk activation but also localized gingival degradation and expression of inflammatory and osteoclastogenic cytokines (**Figure 3**). Intriguingly, stimulation with the TLR2/4 ligand LPS from *P. gingivalis* resulted in a remarkably lower early immune response compared to CpG ODN. A reason for this could be that we employed a one-time topical application of LPS compared to previous studies that injected LPS into the gingival tissue 2-3 times a week [36, 37]. Nevertheless, our study suggests that TLR9 plays an important role in Ctsk-mediated initiation of periodontitis.

The taxonomic composition of the microbial communities colonizing humans and mice was found to differ significantly [38]. While this is not surprising, our 16S rRNA sequencing analysis demonstrated that the mice used in our experiments harbored many of the same genera that are present in the human oral cavity. Interestingly though, more than half of the DNA in both iDNA and eDNA that was recovered from the ligature corresponded to *Enterococcus* and *Staphylococcus*, two genera that were not prominent members of the oral mouse cavity prior to ligature placement (**Figure 5**). These results validate the previously reported mouse oral microbial composition [5] and suggests that ligature-induced periodontitis in mice may not mirror the human oral microbial communities.

eDNA is a structural component of biofilms that stabilizes and shapes the EPS scaffold [39, 40]. In addition, eDNA has a role in bacterial adhesion during the early stages of biofilm formation and maintenance [41, 42], and is thus localized in close contact to the gingival tissue. eDNA is generated by different mechanisms such as lysis of microbes within the biofilm or active release from living cells [43]. Therefore, it is conceivable that the ligature-associated eDNA might represent a mixture of lysed biofilm cells as well as free microbial eDNA from the saliva or other oral sources that could have been trapped in the biofilm accumulated in the ligature.

Although eDNA can clearly be seen as strands between the microbes in human subgingival plaque and recovered ligature from the mouse periodontitis model (**Figure 5**), the function of eDNA in the initiation of periodontitis has not yet been investigated. The present study demonstrated that topical application of human eDNA to the mouse palatal gingiva activated gingival Ctsk. Periodontal microbial DNA has been reported to trigger production of inflammatory mediators in various cell types such as macrophages [44, 45, 46] and gingival fibroblasts [46, 47] through TLR9. The relevance of microbial composition and species responsible for the initiation of periodontitis in humans and mice have been debated as both species harbor distinct microbiomes in their oral cavities. However, if the excreted or secreted microbial eDNA containing consensus unmethylated CpG sequences is involved in the periodontal connective tissue degeneration by Ctsk derived from gingival fibroblasts, the presence of specific microbial species may not be required to the initial pathogenesis of periodontitis (**Figure 5e**).

In conclusion, we report evidence that early disease pathogenesis of periodontitis involves activation of Ctsk secretion from gingival fibroblasts, which is triggered by oral microbial eDNA in dental plaque. We propose that responses of gingival fibroblasts to microbial eDNA leading to secretion of Ctsk into the

connective tissue space are directly implicated in initiating periodontal disease by connective tissue degradation and periodontal pocket formation (**Figure 5e**). Our data suggest a basis for new early disease diagnosis systems and suggests novel therapeutic targets for prevention or treatment of this highly prevalent oral disorder.

Materials And Methods

Animal care

All protocols for animal experiments were reviewed and approved by the University of California Los Angeles (UCLA) Animal Research Committee (ARC# 2003-009) and followed the Public Health Service Policy for the Humane Care and Use of Laboratory Animals and the UCLA Animal Care and Use Training Manual guidelines. C57BL/6J wild type mice (Jackson Laboratory, Bar Harbor, ME) were used in this study. Animals had free access to regular rodent diet and water ad libidum and were maintained in standard housing conditions with 12-hour-light/dark cycles in the Division of Laboratory Animal Medicine at UCLA.

Human Subjects

All protocols involving human subjects were reviewed and approved by the UCLA Institutional Review Board (UCLA-IRB 11-002483). The participants provided verbal informed consent to take part in the study. Saliva samples were collected from 20- to 40-year-old healthy human subjects. Sub-gingival plaque samples were collected from 20- to 40-year-old human subjects with clinical diagnosis of periodontitis. The detailed protocols for further sample processing are described below.

Osteoadsorptive Fluorogenic Substrate Probes

OFS-1 and OFS-3 were synthesized and characterized as described previously[10]. The probes were dissolved in 0.7 mL of 0.9% sodium chloride (NaCl) in water to a concentration of 50 μM and stored at 4 °C in the dark until use.

Evaluation of gingival swelling, alveolar bone resorption and Ctsk activation in a ligature-induced mouse model of periodontitis

A silk thread was gently tied around the left maxillary second molar of 8- to 12-week-old female C57BL6/J wild type mice under general inhalation anesthesia with isoflurane (Henry Schein, Melville, NY). To characterize Ctsk activation, OFS-1 or OFS-3 was prepared and characterized as previously described [15] with minor modifications to further improve yield, and 100 μl of 10 μM OFS prepared in 0.9% NaCl solution was injected through the retro-orbital venous plexus one day prior to euthanasia. At 1, 3, 5 and 7 days after the ligature placement, mice were euthanized by 100% CO_2 inhalation. The maxillary gingival tissues were then digitally photographed and harvested, and the fluorescent signal was measured with the IVIS Spectrum Imaging System (IVIS Lumina II: Perkin Elmer, Waltham, MA). The

gingival swelling area was measured using a Java-based image processing program (ImageJ: NIH, Bethesda, MD) and normalized to the circumferential area of the maxillary second molar. After evaluation of Ctsk using the IVIS, the maxillary bones were harvested from each mouse and fixed in 10% buffered formalin (Thermo Fisher Scientific, Waltham, MA). The fixed maxillary bones were X-rayed at an energy level of 60 kV and 166 μA, and 3D images were reconstructed (Skyscan 1275: Bruker, Billerica, MA). Alveolar bone loss was measured at the middle of the second molar from the cementoenamel junction to the alveolar bone crest. Statistical analysis was performed using two-way analysis of variance with Tukey's multiple comparison test to assess the difference among multiple experimental groups. $P < 0.05$ was considered as statistically significant.

Evaluation of gene expression of *IL-1β*, *IL-6*, *IL-17A* and *RANKL* in a ligature-induced mouse model of periodontitis

At 1, 3, 5 and 7 days after ligature placement, total RNA was extracted from the harvested ligature side or non-ligature side of the maxillary gingival tissues with the RNeasy Mini Kit (QIAGEN, Germantown, MD) and quantified with a Thermo Scientific NanoDrop 1000 ultraviolet-visible spectrophotometer (NanoDrop Technologies, Wilmington, DE). After treatment with DNase I (Thermo Fisher Scientific), cDNA was synthesized from 1 μg of total RNA using Super Script III reverse transcriptase (Super Script VILO: Thermo Fisher Scientific).

Taqman-based qRT-PCR was performed using commercially available primer/probe mixes as follows, *IL-1β* (Mm00434228_m1, Thermo Fisher Scientific), *IL-6* (Mm00446190_m1, Thermo Fisher Scientific), *IL-17A* (Mm00439618_m1, Thermo Fisher Scientific) and *RANKL* (Mm00441908_m1, Thermo Fisher Scientific) in combination with a mouse *GAPDH* internal control mix (Mm99999915_g1, Thermo Fisher Scientific). Target gene expression was quantitatively analyzed using the $\Delta\Delta$CT method. Statistical analysis was performed using Student's *t*-test to assess the difference between the ligature side group and the non-ligature side group at each time point. $P < 0.05$ was considered as statistically significant.

Examination of the function of Ctsk in the initial stage of periodontitis

Following ligature placement, mineral oil (Sigma-Aldrich) alone or supplemented with odanacatib (Selleckchem, Houston, TX) at a dose of 90 μg/100 μl was administered orally once. The gingival swelling area was measured, and the maxillary bones were scanned by microCT at 7 days after ligature placement as described above. Alveolar bone resorption was measured at the middle of the second molar from the cementoenamel junction to the alveolar bone crest. The average of bone area/total area (BV/TV) in the alveolar bone on the buccal and palatal side of the second molar was measured from the apex of the root to the cementoenamel junction. The harvested maxillae with gingival tissue at 1, 3 and 7 days after ligature placement were fixed in 10% buffered formalin (Thermo Fisher Scientific, Waltham, MA) and decalcified in 10% EDTA (Sigma-Aldrich, Saint Louis, MO) for 3 weeks. After the decalcification, samples were embedded in paraffin. Paraffin sections (4 μm) were immunohistochemically stained for Ctsk and counterstained with methylene blue, prior to staining with hematoxylin and eosin (HE). The paraffin sections of the maxillas at 7 days after ligature placement were also stained with

picrosirius red (PolyScience, Niles, IL). The collagen fiber structure of the gingival connective tissue and periodontal ligament was evaluated using confocal laser scanning microscopy (SP8: Leica Microsystems, Wetzlar, Germany). Picrosirius red was visualized via excitation with a 20 mW DPSS 561 nm and emission collection at 635-685 nm bandwidth. The connective tissue area was measured (ImageJ) and normalized to the area between tooth surface and the surface of the alveolar bone. Statistical analysis was performed using Student's *t*-test to assess the difference between the experimental groups. $P < 0.05$ was considered as statistically significant.

Evaluation of steady state gene expression profiles in a ligature-induced mouse model of periodontitis by scRNA-seq

At 1 day after ligature placement, the maxillary gingival tissues were harvested from freshly isolated mouse maxillae.

Collagenase II treatment: The tissues were cut into about 1 mm^2 pieces and placed immediately into 20 ml digestion buffer containing 1 mg/ml collagenase II (Life Technologies, Grand Island, NY), 10 units/ml DNase I (Sigma-Aldrich) and 1% bovine serum albumin (BSA; Sigma-Aldrich) in Dulbecco's modified Eagle's medium (DMEM; Life Technologies). The chopped tissues were incubated in the digestion buffer for 20 minutes at 37 ºC on a 150 rpm shaker. The tissues were then passed through a 70 µm cell strainer, pelleted at 1,500 rpm for 10 minutes at 4 ºC before being resuspended in phosphate-buffered saline (PBS; Life Technologies) that was supplemented with 0.04% BSA (Cell suspension A) and counted to generate "Cell suspension A".

Trypsin treatment: The parts of the tissues that did not pass through the 70 µm cell strainer after collagenase II treatment, were subjected to additional incubation in 10 ml of 0.25% trypsin (Life Technologies) and 10 units/ml DNase I for 30 minutes at 37 ºC on a 150 rpm shaker. Trypsin was neutralized with 10 ml of fetal bovine serum (FBS; Life Technologies), and the tissues were passed through a 70 µm cell strainer, which was washed with 10 ml DMEM. The collected cells were then pelleted at 1,500 rpm for 10 minutes at 4 ºC, resuspended in PBS that was supplemented with 0.04% BSA and counted to generate "Cell suspension B".

Cell suspension A and Cell suspension B were combined into one tube for scRNA-seq (10X Genomics, San Francisco, CA). The Cell Ranger output of scRNA-seq data was analyzed using an R toolkit for single cell genomics (Seurat, https://satijalab.org/seurat/).

Evaluation of Ctsk activation and gingival swelling by topical application of cultured oral biofilm or planktonic bacteria

Saliva samples from 20- to 40-year-old healthy human subjects were collected and diluted to 25% with PBS. The diluted saliva was centrifuged at 2,600 g for 10 minutes to pellet large debris and eukaryotic cells. Prior to seeding of the oral biofilm, 100 µl of the diluted saliva was grown in 1ml of SHI medium [48] for 17-18 hours under anaerobic conditions (10% CO_2, 10% H_2 and 80% N_2). This overnight grown oral

microbial community was pelleted and washed with PBS. For biofilm seeding, cells were diluted cells to an optical density at 600 nm of 0.1 into 100% SHI medium supplemented with 5 mM $CaCl_2$. Further, 1 ml of this diluted oral community was seeded onto oral appliances which were custom-made of clear dental resin (GC America, Alsip, IL) and incubated under anaerobic conditions at 37 ºC for 5 days. Cultured oral community was treated with 10 U/ml DNase I and resuspended in PBS to prepare a planktonic bacteria solution free of extracellular polymeric substances including eDNA.

The palates were covered by an oral appliance with cultured oral biofilm, or three µl of planktonic bacteria solution (3×10^7 CFU) were topically applied to the palate and the palates were covered by an oral appliance. After 1 hour of covering the palate, the oral appliances were removed. One hundred µl of 10 µM OFS solution was injected through the retro-orbital venous plexus one day prior to euthanasia. At 4 days after the topical application of cultured oral biofilm or planktonic bacteria, the fluorescent signal was measured, and the gingival swelling area was measured and normalized to the whole area of the palate. Statistical analysis was performed using two-way analysis of variance with Tukey's multiple comparison test to assess the difference among multiple experimental groups. $P < 0.05$ was considered as statistically significant.

Evaluation of Ctsk activation and gingival swelling by topical application of CpG DNA or LPS

Three µl of 1 µg/ml of CpG ODN (InvivoGen, San Diego, CA), 1 µg/ml of LPS from *P. gingivalis* (InvivoGen) or 1 µg/ml of control ODN (InvivoGen) were topically applied to the palate as described above, and 100 µl of 10 µM OFS solution was injected through the retro-orbital venous plexus one day prior to euthanasia. At 4 days after the topical application of CpG ODN, *P. gingivalis* LPS or control ODN, the fluorescent signal was measured, and the gingival swelling area was measured and normalized to the whole area of the palate. Statistical analysis was performed using two-way analysis of variance with Tukey's multiple comparison test to assess the difference among multiple experimental groups. $P < 0.05$ was considered as statistically significant. In addition, the harvested maxillas were immunohisto-stained for Ctsk and stained with HE as described above.

Evaluation of gene expression of *IL-6* and *IL-17A* in mouse gingival tissues with topical application of CpG DNA

At 4 days after the topical application of CpG ODN or control ODN, total RNA was extracted from the maxillary gingival tissues, and RT qPCR was synthesized as described above. Statistical analysis was performed using Student's *t*-test to assess the difference between the experimental groups. $P < 0.05$ was considered as statistically significant.

Evaluation of steady state gene expression profiles in mouse gingival tissues with topical application of CpG DNA or LPS by scRNA-seq

At 4 days after the palatal topical application of CpG ODN or *P. gingivalis* LPS, the maxillary gingival tissues were harvested from freshly isolated mouse maxillas. Single cells were dissociated from the

maxillary gingival tissues, and scRNA-seq was performed as described above.

Evaluation of gene expression of *TLR9* in gingival fibroblasts and skin fibroblasts

Primary gingival fibroblasts or skin fibroblasts from 8- to 12-week-old female wild type mice were cultured using an explant method as previously reported [49]. The cells were cultured in DMEM with 10% FBS and 100 U penicillin/0.1 mg/ml streptomycin (Life Technologies) at 37 ºC, 5% CO_2 in a humidified incubator.

Total RNA was extracted from the gingival fibroblasts or skin fibroblasts, and cDNA was synthesized as described above. Taqman-based qRT-PCR was performed using a commercially available primer/probe mix for *TLR9* (Mm00446193_m1, Thermo Fisher Scientific). Statistical analysis was performed using Student's *t*-test to assess the difference between the experimental groups. $P < 0.05$ was considered as statistically significant.

Evaluation of induction of Ctsk secretion or production of Ctsk protein in gingival fibroblasts by CpG DNA

Primary mouse gingival fibroblasts were cultured in DMEM supplemented with 10% FBS and 100 U penicillin/0.1 mg/ml streptomycin in the presence of 0, 0.1, 1 or 10 μg/ml of CpG ODN at 37 ºC, 5% CO_2 in a humidified incubator for 24 hours.

Culture supernatant or cell solution lysed with RIPA Lysis and Extraction buffer (VWR, Radnor, PA, USA) supplemented with a protease and phosphatase inhibitor cocktail (Thermo Fisher Scientific). The Ctsk protein concentration in the culture supernatant or lysed cell solution was determined by a colorimetric method (OD at 450 nm) using a Ctsk ELISA kit (MyBioSource, San Diego, CA, USA). Statistical analysis was performed using two-way analysis of variance with Tukey's multiple comparison test to assess the difference among multiple experimental groups. $P < 0.05$ was considered as statistically significant.

Extraction of iDNA or eDNA from a human saliva-derived oral microbial community

Extracellular (eDNA) and intracellular DNA (iDNA) were extracted from human saliva-derived biofilms. After biofilm growth in 100% SHI medium supplemented with 5 mM $CaCl_2$ under anaerobic conditions at 37 ºC for 5 days, planktonic cells were removed by gently aspirating the medium and carefully washing once with 500 μl PBS. Following the wash, 250 μl of PBS was added in each well, and microbial cells were harvested by scraping and pipetting with a sterile pipette tip. The bacterial cells were then transferred to an Eppendorf tube and pelleted at 3,250 g for 15 minutes at 4°C for DNA isolation. The supernatant was filtered through 0.22 μm syringe filters to exclude bacterial cells. While the bacterial pellet was used for iDNA isolation, the cell- free supernatant was further processed for eDNA isolation.

iDNA extraction: The bacterial pellet was used for iDNA extraction using the Epicentre MasterPure DNA extraction and Purification Kit (Lucigen, Middleton, WI) according to the manufacturer's instructions [50].

eDNA extraction: eDNA was extracted from the cell free supernatants of the microbial biofilm according to a previously described protocol [51]. Briefly, the cell-free supernatants (containing eDNA) were mixed

with 2 volumes of absolute ethanol and a 1/10th volume of sodium acetate (3 M, pH 5.2) containing 1 mM EDTA. After overnight precipitation at -80°C, eDNA was pelleted by centrifugation at 13,000 rpm at 4°C for 20 minutes followed by a wash with ice-cold 70% ethanol. The eDNA was then air dried, dissolved in sterile deionized water and quantified using NanoDrop.

Evaluation of Ctsk activation and gingival swelling by topical application of eDNA or iDNA

Three µl of 1 µg/ml solution of eDNA or iDNA were topically applied to the palate as described above, and 100 µl of 10 µM OFS solution was injected through the retro-orbital venous plexus one day prior to euthanasia. At 4 days after the topical application of eDNA or iDNA, the fluorescent signal was measured, and the gingival swelling area was measured and normalized to the whole area of the palate. Statistical analysis was performed using two-way analysis of variance with Tukey's multiple comparison test to assess the difference among multiple experimental groups. $P < 0.05$ was considered as statistically significant.

Evaluation of eDNA and iDNA of mouse oral biofilm harvested from recovered ligatures

The ligatures were recovered from the mouse model of periodontitis 1 day (n = 4) and 7 days (n = 4) after placement. iDNA and eDNA samples were prepared separately as above and subjected to 16S rRNA sequencing of the V4 region (Laragen, Inc, Culver City, CA). Demultiplexed sequences were imported into Qiime 2 (v2020.11). Low quality sequences containing bases with Phred quality values <20 were trimmed and denoised using the DADA2 package [52]. The amplicon sequence variants (ASVs) generated after the denoising were taxonomically assigned by comparison to the HOMD database.

SYTOX Green staining of the subgingival plaque from a periodontitis patient and the recovered ligature.

Subgingival plaque was collected from a periodontitis patient and stained with SYTOX Green (Thermo Fisher Scientific). The eDNA scaffold in the plaque was evaluated via fluorescence microscopy (Zeiss Axio Imager M2 with Zen 2.5 pro software). Sytox green was visualized using epifluorescence through a 100x/1.4 Plan Achromat objective at 450 to 490 nm bandwidth excitation and 500 to 550 nm bandwidth emission filters. The recovered ligature from the mouse periodontitis model was stained with SYTOX Orange and was visualized similarly but with 538 to 562 nm bandwidth excitation and 570 to 640 nm bandwidth emission filter settings.

Declarations

Acknowledgements

This investigation was supported by NIH grants R21DE023410, R44DE025524 and C06RR014529, SINTX Technologies and by the USC Dornsife Bridge Institute.

Author contributions

I.N., R.L, and C.E.M. designed and supervised the study. Y.Z. and O.S. synthesized OFS, which was designed by C.E.M.. T.K., H.O., A.H. and I.N. performed animal studies. T.K. performed scRNA-seq, *in vitro* studies and data analysis. B.S. performed human oral microbial culture, bacterial DNA extraction and sequencing analysis. T.K. and I.N. drafted the manuscript, which was critically reviewed and revised by R.L. and C.E.M. All authors gave final approval and agreed to be accountable for all aspects of the work.

Competing interests

I.N. is consultant for FUJIFILM Corp and BioVinc, LLC., and received funding from SINTX Technologies. C.E.M. is a founding member and equity holder of BioVinc, LLC. All other authors report no competing interests.

Data availability statement

We state where data supporting the results reported in a published article can be found, including, where applicable, hyperlinks to publicly archived datasets analyzed or generated during the study. Single cell RNA sequence data are available at GEO.

References

1. Eke PI, Thornton-Evans GO, Wei L, Borgnakke WS, Dye BA, Genco RJ. Periodontitis in US Adults: National Health and Nutrition Examination Survey 2009-2014. *J Am Dent Assoc* **149**, 576-588 e576 (2018).

2. Marcenes W*, et al.* Global burden of oral conditions in 1990-2010: a systematic analysis. *J Dent Res* **92**, 592-597 (2013).

3. Hienz SA, Paliwal S, Ivanovski S. Mechanisms of Bone Resorption in Periodontitis. *J Immunol Res* **2015**, 615486 (2015).

4. Bunte K, Beikler T. Th17 Cells and the IL-23/IL-17 Axis in the Pathogenesis of Periodontitis and Immune-Mediated Inflammatory Diseases. *Int J Mol Sci* **20**, (2019).

5. Dutzan N*, et al.* A dysbiotic microbiome triggers TH17 cells to mediate oral mucosal immunopathology in mice and humans. *Sci Transl Med* **10**, (2018).

6. Hajishengallis G. New developments in neutrophil biology and periodontitis. *Periodontol 2000* **82**, 78-92 (2020).

7. Rams TE, Listgarten MA, Slots J. Radiographic alveolar bone morphology and progressive periodontitis. *J Periodontol* **89**, 424-430 (2018).

8. Donos N. The periodontal pocket. *Periodontol 2000* **76**, 7-15 (2018).

9. Kononen E, Gursoy M, Gursoy UK. Periodontitis: A Multifaceted Disease of Tooth-Supporting Tissues. *J Clin Med* **8**, (2019).

10. Kinane DF, Stathopoulou PG, Papapanou PN. Periodontal diseases. *Nat Rev Dis Primers* **3**, 17038 (2017).

11. Takata T, Donath K. The mechanism of pocket formation. A light microscopic study on undecalcified human material. *J Periodontol* **59**, 215-221 (1988).

12. Divieti Pajevic P, Krause DS. Osteocyte regulation of bone and blood. *Bone* **119**, 13-18 (2019).

13. Feng H*, et al.* Tendon-derived cathepsin K-expressing progenitor cells activate Hedgehog signaling to drive heterotopic ossification. *J Clin Invest* **130**, 6354-6365 (2020).

14. Donners MM*, et al.* Cathepsin K Deficiency Prevents the Aggravated Vascular Remodeling Response to Flow Cessation in ApoE-/- Mice. *PLoS One* **11**, e0162595 (2016).

15. Richard ET*, et al.* Design and Synthesis of Cathepsin-K-Activated Osteoadsorptive Fluorogenic Sentinel (OFS) Probes for Detecting Early Osteoclastic Bone Resorption in a Multiple Myeloma Mouse Model. *Bioconjug Chem* **32**, 916-927 (2021).

16. Abe T, Hajishengallis G. Optimization of the ligature-induced periodontitis model in mice. *J Immunol Methods* **394**, 49-54 (2013).

17. Drake MT, Clarke BL, Oursler MJ, Khosla S. Cathepsin K Inhibitors for Osteoporosis: Biology, Potential Clinical Utility, and Lessons Learned. *Endocr Rev* **38**, 325-350 (2017).

18. Hao L*, et al.* Odanacatib, A Cathepsin K-Specific Inhibitor, Inhibits Inflammation and Bone Loss Caused by Periodontal Diseases. *J Periodontol* **86**, 972-983 (2015).

19. Flemming HC, Wingender J, Szewzyk U, Steinberg P, Rice SA, Kjelleberg S. Biofilms: an emergent form of bacterial life. *Nat Rev Microbiol* **14**, 563-575 (2016).

20. Akira S. Innate immunity to pathogens: diversity in receptors for microbial recognition. *Immunol Rev* **227**, 5-8 (2009).

21. Kang JY*, et al.* Recognition of lipopeptide patterns by Toll-like receptor 2-Toll-like receptor 6 heterodimer. *Immunity* **31**, 873-884 (2009).

22. Chukkapalli SS*, et al.* Impaired innate immune signaling due to combined Toll-like receptor 2 and 4 deficiency affects both periodontitis and atherosclerosis in response to polybacterial infection. *Pathog Dis* **76**, (2018).

23. Crump KE, Sahingur SE. Microbial Nucleic Acid Sensing in Oral and Systemic Diseases. *J Dent Res* **95**, 17-25 (2016).

24. Moutsopoulos NM, Konkel JE. Tissue-Specific Immunity at the Oral Mucosal Barrier. *Trends Immunol* **39**, 276-287 (2018).

25. Hirai T*, et al.* Cathepsin K is involved in development of psoriasis-like skin lesions through TLR-dependent Th17 activation. *J Immunol* **190**, 4805-4811 (2013).

26. Hasan M, Gruber E, Cameron J, Leifer CA. TLR9 stability and signaling are regulated by phosphorylation and cell stress. *J Leukoc Biol* **100**, 525-533 (2016).

27. Whitchurch CB, Tolker-Nielsen T, Ragas PC, Mattick JS. Extracellular DNA required for bacterial biofilm formation. *Science* **295**, 1487 (2002).

28. Yamaza T, Goto T, Kamiya T, Kobayashi Y, Sakai H, Tanaka T. Study of immunoelectron microscopic localization of cathepsin K in osteoclasts and other bone cells in the mouse femur. *Bone* **23**, 499-509 (1998).

29. Yamalik N, Gunday S, Kilinc K, Karabulut E, Berker E, Tozum TF. Analysis of cathepsin-K levels in biologic fluids from healthy or diseased natural teeth and dental implants. *Int J Oral Maxillofac Implants* **26**, 991-997 (2011).

30. Garg G, Pradeep AR, Thorat MK. Effect of nonsurgical periodontal therapy on crevicular fluid levels of Cathepsin K in periodontitis. *Arch Oral Biol* **54**, 1046-1051 (2009).

31. Hao L*, et al.* Deficiency of cathepsin K prevents inflammation and bone erosion in rheumatoid arthritis and periodontitis and reveals its shared osteoimmune role. *FEBS Lett* **589**, 1331-1339 (2015).

32. Beklen A, Al-Samadi A, Konttinen YT. Expression of cathepsin K in periodontitis and in gingival fibroblasts. *Oral Dis* **21**, 163-169 (2015).

33. Flemming HC, Wingender J. The biofilm matrix. *Nat Rev Microbiol* **8**, 623-633 (2010).

34. Darveau RP*, et al.* Porphyromonas gingivalis lipopolysaccharide contains multiple lipid A species that functionally interact with both toll-like receptors 2 and 4. *Infect Immun* **72**, 5041-5051 (2004).

35. Kim PD, Xia-Juan X, Crump KE, Abe T, Hajishengallis G, Sahingur SE. Toll-Like Receptor 9-Mediated Inflammation Triggers Alveolar Bone Loss in Experimental Murine Periodontitis. *Infect Immun* **83**, 2992-3002 (2015).

36. Li Y, Lu Z, Zhang L, Kirkwood KL, Lopes-Virella MF, Huang Y. Acid sphingomyelinase deficiency exacerbates LPS-induced experimental periodontitis. *Oral Dis* **26**, 637-646 (2020).

37. Suh JS, Kim S, Bostrom KI, Wang CY, Kim RH, Park NH. Periodontitis-induced systemic inflammation exacerbates atherosclerosis partly via endothelial-mesenchymal transition in mice. *Int J Oral Sci* **11**, 21 (2019).

38. Chun J, Kim KY, Lee JH, Choi Y. The analysis of oral microbial communities of wild-type and toll-like receptor 2-deficient mice using a 454 GS FLX Titanium pyrosequencer. *BMC Microbiol* **10**, 101 (2010).

39. Schilcher K, Horswill AR. Staphylococcal Biofilm Development: Structure, Regulation, and Treatment Strategies. *Microbiol Mol Biol Rev* **84**, (2020).

40. Costa OYA, Raaijmakers JM, Kuramae EE. Microbial Extracellular Polymeric Substances: Ecological Function and Impact on Soil Aggregation. *Front Microbiol* **9**, 1636 (2018).

41. Devaraj A*, et al.* The extracellular DNA lattice of bacterial biofilms is structurally related to Holliday junction recombination intermediates. *Proc Natl Acad Sci U S A* **116**, 25068-25077 (2019).

42. Jakubovics NS, Burgess JG. Extracellular DNA in oral microbial biofilms. *Microbes Infect* **17**, 531-537 (2015).

43. Sanchez-Torres V, Hu H, Wood TK. GGDEF proteins YeaI, YedQ, and YfiN reduce early biofilm formation and swimming motility in Escherichia coli. *Appl Microbiol Biotechnol* **90**, 651-658 (2011).

44. Sahingur SE, Xia XJ, Schifferle RE. Oral bacterial DNA differ in their ability to induce inflammatory responses in human monocytic cell lines. *J Periodontol* **83**, 1069-1077 (2012).

45. Sahingur SE, Xia XJ, Alamgir S, Honma K, Sharma A, Schenkein HA. DNA from Porphyromonas gingivalis and Tannerella forsythia induce cytokine production in human monocytic cell lines. *Mol Oral Microbiol* **25**, 123-135 (2010).

46. Nonnenmacher C, Dalpke A, Zimmermann S, Flores-De-Jacoby L, Mutters R, Heeg K. DNA from periodontopathogenic bacteria is immunostimulatory for mouse and human immune cells. *Infect Immun* **71**, 850-856 (2003).

47. Wara-aswapati N*, et al.* Induction of toll-like receptor expression by Porphyromonas gingivalis. *J Periodontol* **84**, 1010-1018 (2013).

48. Tian Y*, et al.* Using DGGE profiling to develop a novel culture medium suitable for oral microbial communities. *Mol Oral Microbiol* **25**, 357-367 (2010).

49. Glass D*, et al.* Gene expression changes with age in skin, adipose tissue, blood and brain. *Genome Biol* **14**, R75 (2013).

50. Agnello M*, et al.* Microbiome Associated with Severe Caries in Canadian First Nations Children. *J Dent Res* **96**, 1378-1385 (2017).

51. Liao S*, et al.* Streptococcus mutans extracellular DNA is upregulated during growth in biofilms, actively released via membrane vesicles, and influenced by components of the protein secretion machinery. *J Bacteriol* **196**, 2355-2366 (2014).

52. Callahan BJ, McMurdie PJ, Rosen MJ, Han AW, Johnson AJA, Holmes SP. DADA2: high-resolution sample inference from Illumina amplicon data. *Nature methods* **13**, 581-583 (2016).

Figures

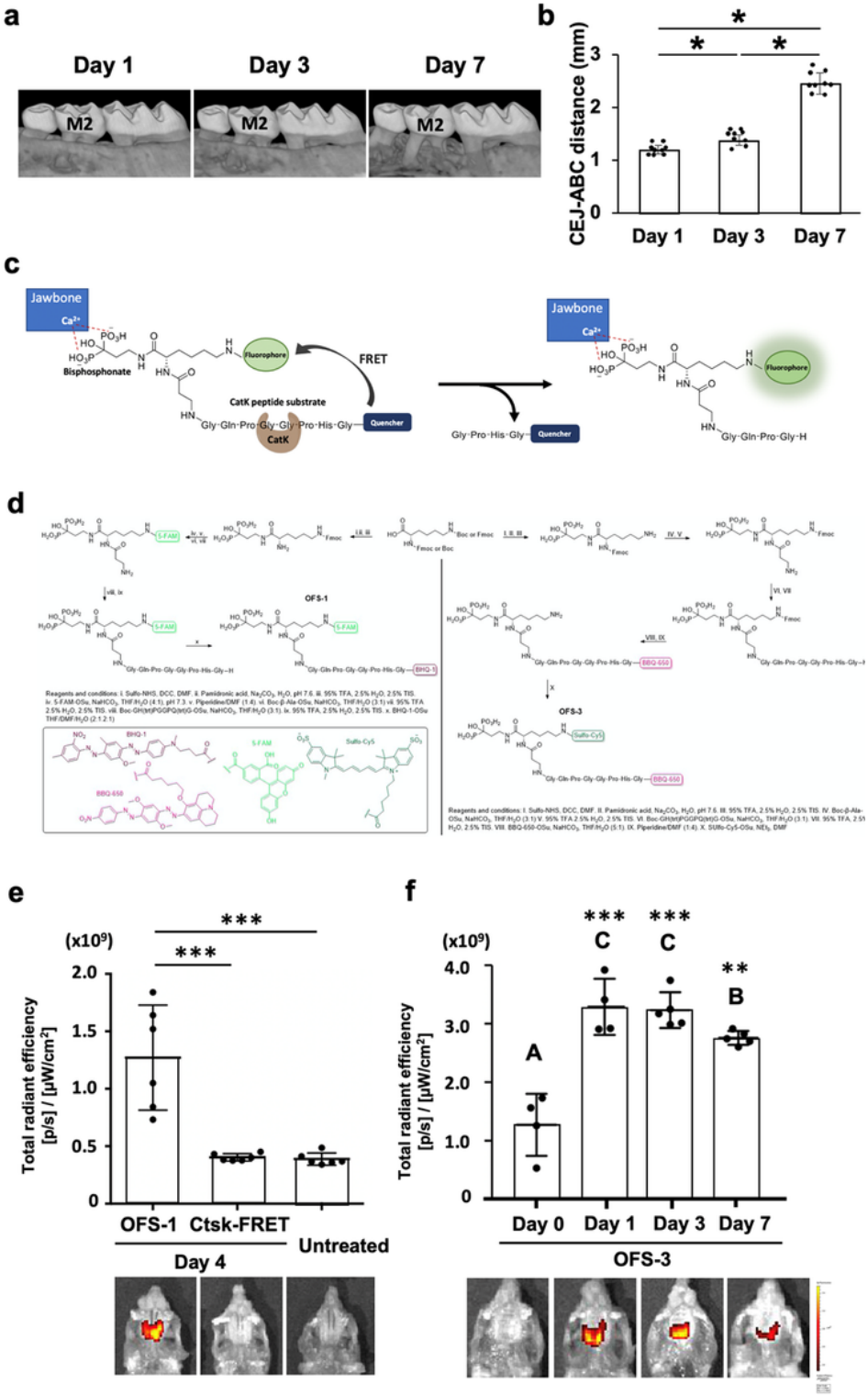

Figure 1

Early cathepsin K (Ctsk) activation in the ligature-induced periodontitis in mice.

a. The ligature (5.0 silk suture) was placed around the maxillary second molar (M2). Representative micro-CT images of the maxilla taken from the lateral view at the 1, 3 and 7 days after ligature placement. **b**. Alveolar bone loss was measured at the middle of the second molar from cementoenamel junction (CEJ) to the alveolar bone crest (ABC) (n = 9). **c**. The Osteoadsorptive Fluorogenic Sentinel (OFS) probe. OFS binds strongly to bone, where it remains quenched until activation by Ctsk through cleavage of a linker region containing the CtsK substrate motif. **d**. Chemical synthesis scheme of OFS-1 with 5-FAM / BHQ-1 and OFS-3 with Sulfo-Cy5 / BBQ-650. (Adapted from [15]) **e**. Day 4 of ligature placement, OFS-1 signal was detected but the fluorescent signal was not detected from a commercially available Ctsk FRET probe without a bisphosphonate bone anchoring element (SensoLyte 520, Anaspec, Remont, CA). **f**. Representative images showing Ctsk activation of OFS-3 fluorescence detected by an IVIS Spectrum system at 0, 1, 3 and 7 days after ligature placement. Quantification of the fluorescent signal was performed by region-of-interest placement to capture the entire palate, and results were represented as the total fluorescent signal (n = 4-5). ANOVA with Tukey's multiple-comparison test (**b**, **F**) and Student's *t*-test (**e**). Data are presented as mean values ± SD; *$p < 0.05$, **p<0.01; ***p<0.0001. Different characters (A-B, B-C, A-C) indicate statistically significant differences.

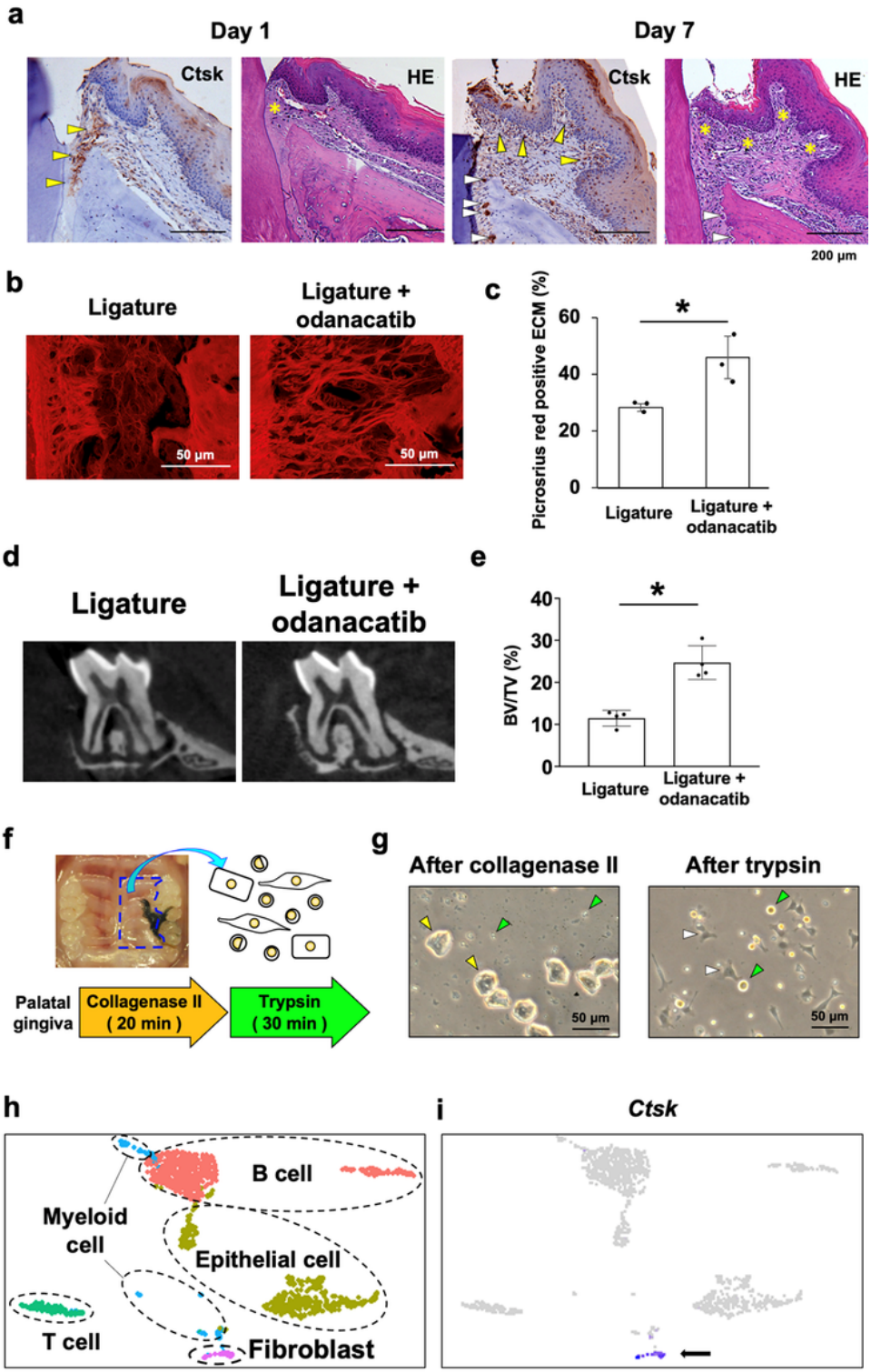

Figure 2

The pathological role of Ctsk and its cellular source in mouse gingiva.

a. Immunohistochemical staining for Ctsk, counterstaining with methylene blue, and HE staining of the periodontal tissue at the 1 and 7 days after ligature placement (scale bars: 200 μm). *Yellow arrows* indicate the Ctsk positive cells in the gingival and periodontal ligament connective tissue. *White arrows*

indicate the Ctsk positive osteoclasts on the alveolar bone and osteoclastic lacunae. *Yellow asterisks* indicate disintegrated gingival connective tissue. **b**. Representative fluorescent picrosirius red images of the gingival connective tissue and periodontal ligament at 7 days after ligature placement with or without administration of the Ctsk inhibitor odanacatib (scale bars: 50 μm). **c**. The picrosirius-stained collagen structure in the periodontal ligament connective tissue area was measured as percentage of the area between tooth surface and the surface of alveolar bone (n = 3). **d.** Representative micro-CT cross-sectional images of second molar 7 days after ligature placement with or without odanacatib administration. **e**. The average bone volume/total volume (BV/TV) in the alveolar bone on the buccal and palatal side of the second molar as measured from the apex of the root to the cementoenamel junction (n = 4). **f.** Single cell dissociation method for the ligature side of the palate at 1 day after ligature placement. **g.** Phase contrast images of dissociated cells after collagenase II treatment and trypsin treatment (scale bars: 50 μm). *Yelllow arrows* indicate epithelial cells. *Green arrows* indicate immune cells. *White arrows* indicate fibroblasts. **h**. Single cell RNA sequencing (scRNA-seq) *t*-SNE projection plots showing major classes of dissociated cells at 1 day after ligature placement. Colors indicate cell type (*Red*: B cell, *yellow*: epithelial cell, *green*: T cell, *blue*: myeloid cell, *pink*: fibroblast). **i**. scRNA-seq *t*-SNE projection plots showing transcript accumulation for *Ctsk* genes predominantly in fibroblasts (arrow). Student's *t*-test (**c, e**). Data are presented as mean values ± SD; *$p < 0.05$

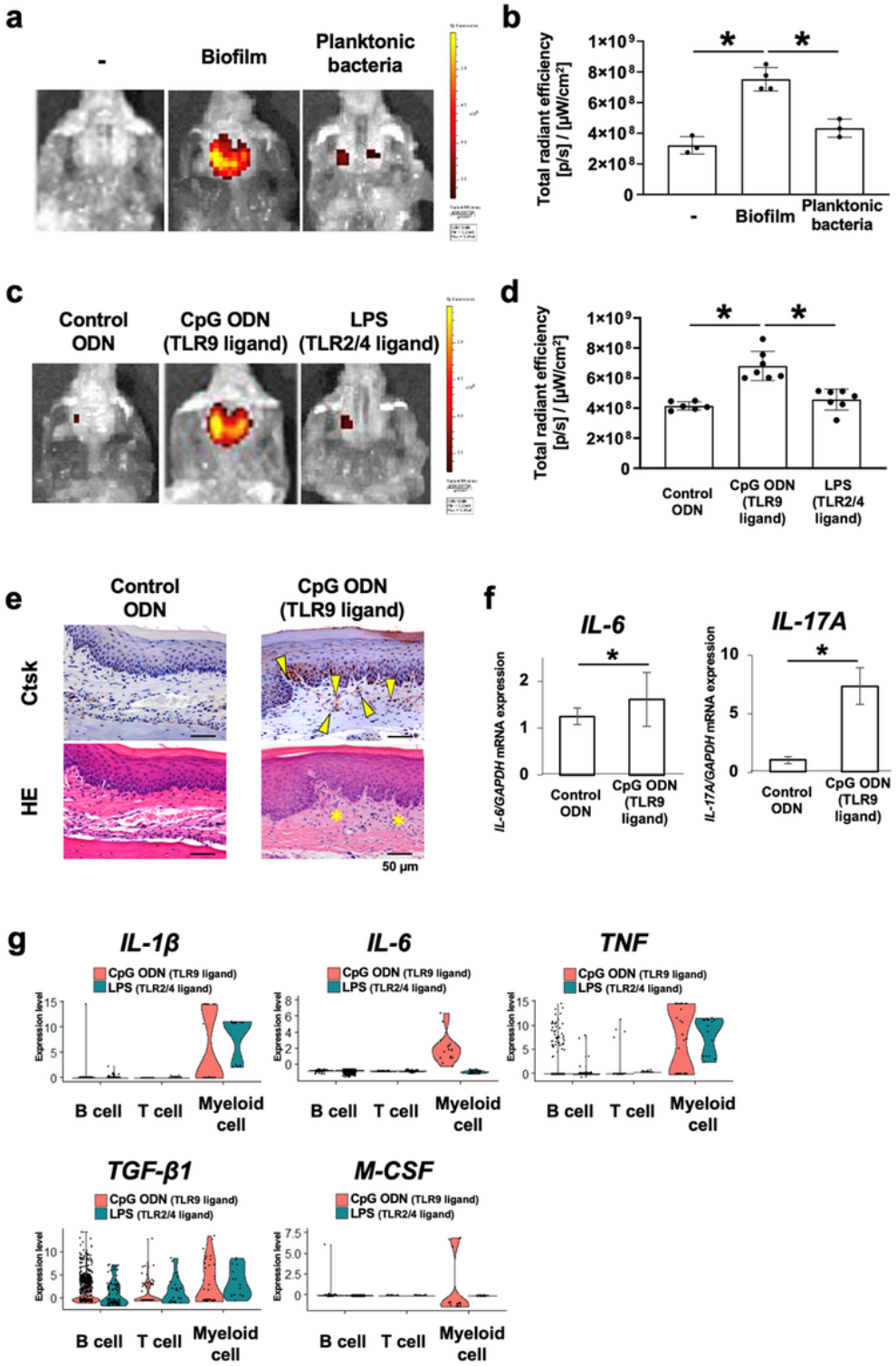

Figure 3

Topical application of human oral biofilm and biofilm components to activate Ctsk in palatal tissue of mice.

a. Cultured human oral microbial biofilm or planktonic bacteria were topically applied to the mouse palatal gingiva for 1 hr covered by an oral appliance (Figure S5). OFS-1 was IV injected 3 days after the

topical application of human microbial samples and 24 hr later, the Ctsk activation was detected by OFS-1 fluorescence. **b.** Quantification of the OFS-1 fluorescent signal at 4 days after topical application of cultured oral microbial biofilms or planktonic bacteria to the palate (n = 3-4). **C**. Representative images showing OFS-1-derived fluorescent signal 4 days after the topical application of control ODN, CpG ODN (TLR9 ligand) or LPS (TLR2/4 ligand) solution to the palatal gingiva (n = 6-7). **d**. Quantification of the OFS-1 fluorescent signal after topical application of control ODN, CpG ODN or LPS to the mouse palatal gingiva. **e.** Immunohistochemical staining for Ctsk and HE staining of the periodontal tissue at 4 days after topical application of control ODN or CpG ODN (scale bars: 50 μm). *Yellow arrows* indicate Ctsk positive cells in the connective tissue. *Yellow asterisks* indicate the disintegrated gingival connective tissue. **f.** RT qPCR of *IL-6* and *IL-17A* on the palatal gingival tissue at 4 days after topical application of control ODN or CpG ODN solution was determined by quantitative real-time RT-PCR analysis (n = 3). **g**. scRNA-seq violin plots showing gene expression levels of *IL-1β*, *IL-6*, *TNF*, *TGF-β1* and *M-CSF* in B cells, T cells and myeloid cells which were collected from the palatal gingival tissue 4 days after topical application of CpG ODN or LPS solution. ANOVA with Tukey's multiple-comparison test (**b, d**) and Student's *t*-test (**f**). Figure presented as mean values ± SD; *$p < 0.05$.

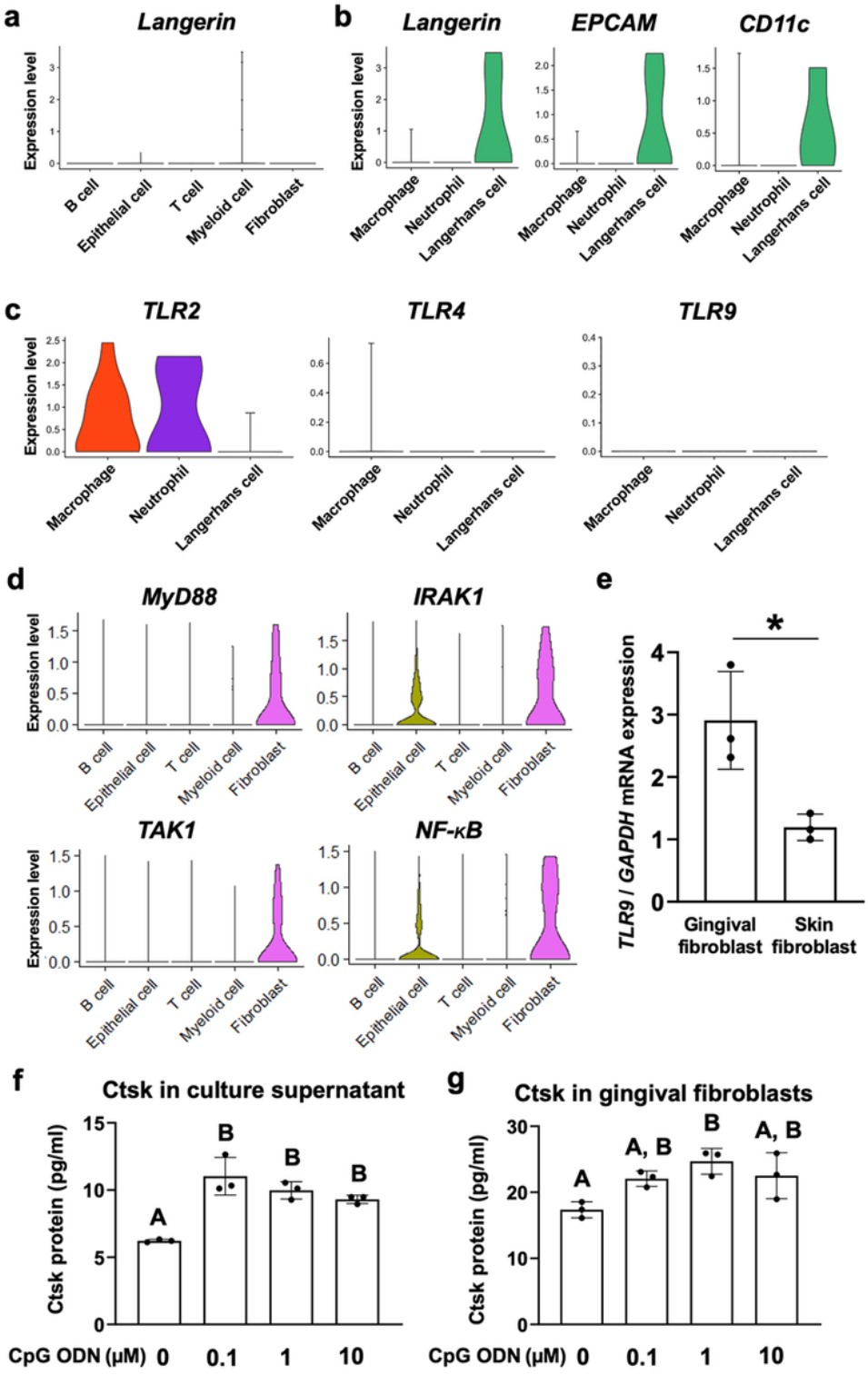

Figure 4

TLR9 in gingival immune cells and fibroblasts

a. Analysis of scRNA-seq of Day 1 gingival cells identified *Langerin* expressing Langerhans cells in the myeloid cell cluster. **b**. The myeloid cell cluster was subclustered. One subcluster was associated with the selective expression of *Langerin*, *Epcam* and *CD11c* and thus designated as Langerhans cells. **c**. Myeloid

cell subclusters exhibited the expression of *TLR2* and *TLR4* at different degrees. However, the *TLR9* expression was not detected by scRNA-seq. **d**. TLR-related gene expression in gingival cells harvested 1 day after the ligature placement. scRNA-seq violin plots showing gene expression level of *MyD88*, *IRAK1*, *TAK1* and *NF-$_K$B* predominantly in fibroblasts. **e**. Gene expression of *TLR9* in gingival fibroblasts and skin fibroblasts was determined by quantitative real-time RT-PCR analysis (n = 3). **f.** Ctsk in supernatant of mouse gingival fibroblast culture with CpG ODN supplementation determined by ELISA (n = 3). **g**. Ctsk in the cultured gingival fibroblast with CpG ODN supplementation determined by ELISA (n = 3). Student's *t*-test (**E**) and ANOVA with Tukey's multiple-comparison test (**f** and **g**). Data are presented as mean values ± SD; *$p < 0.05$. Different characters (A-B) indicate statistically significant differences ($p < 0.05$).

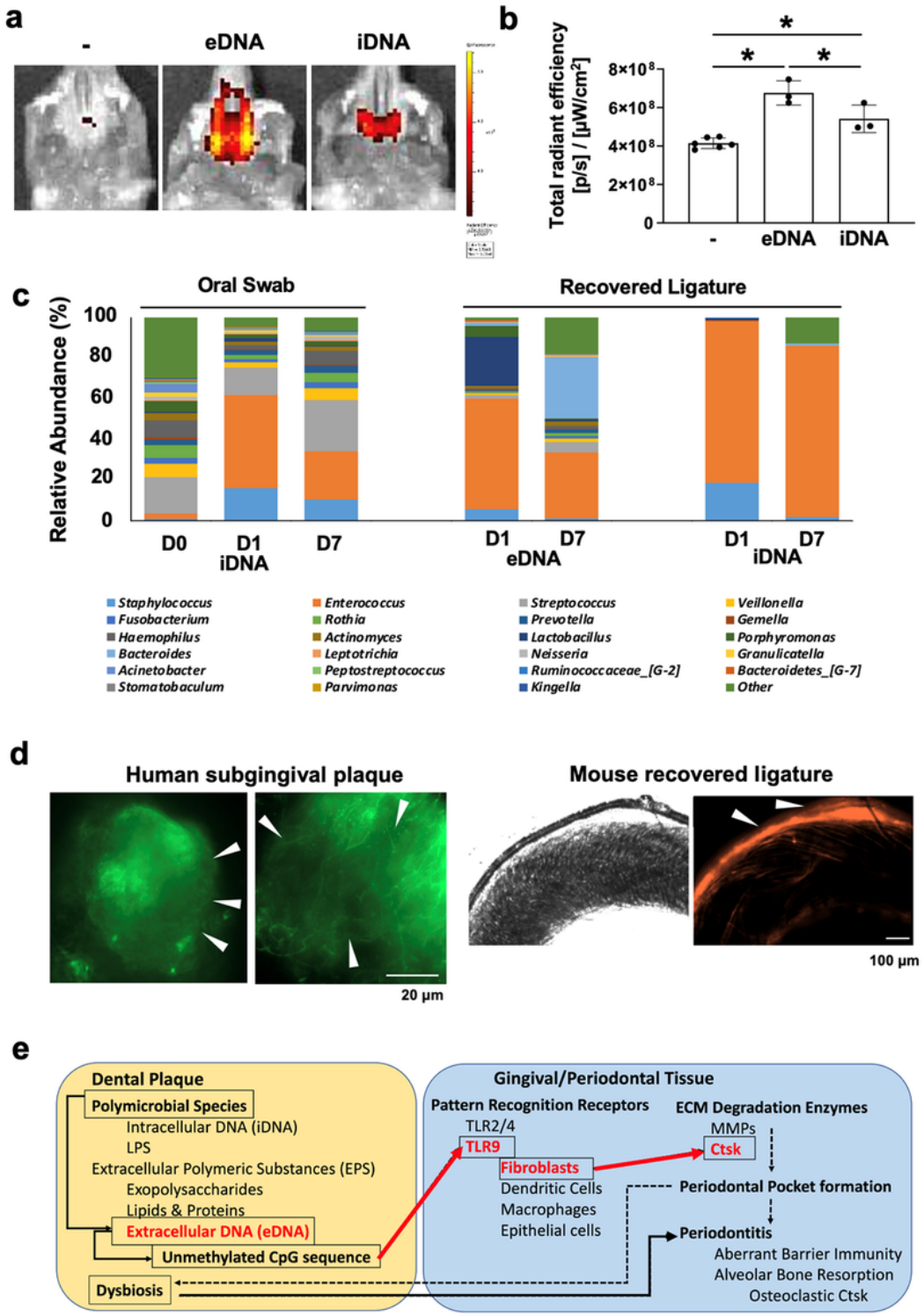

Figure 5

Microbial extracellular DNA (eDNA) is a potent activator of gingival Ctsk.

a. OFS-1 was IV injected 3 days after the 1-hr topical application of eDNA or iDNA to the mouse palatal gingiva and the fluorescent signal was recorded 4 days after the eDNA or iDNA topical application. **b.** Quantification of OFS-1 fluorescent signal (n = 3-6). **c.** Relative abundance of microbial genera in the

mouse periodontitis model. The palatal gingival swabs were collected at before (D0), 1 day (D1) and 7 days (D7) after ligature placement (n=3 per time point). The ligatures were recovered from the mouse maxillary second molar D1 and D7 (n=4 per time point). eDNA and iDNA samples were prepared (n=4 per sample that were combined) and subjected to 16S rRNA sequencing. **d**. SYTOX-green-fluorescent images of subgingival plaque collected from human subjects with clinically diagnosed periodontitis (scale bar: 20 μm) and a pair of incident-light and SYTOX-orange-fluorescent images of a recovered ligature from the mouse periodontitis model. *Arrowheads* indicate eDNA. **e**. The proposed mechanism of periodontitis initiation (red letters and arrows). The present study indicated that eDNA component of the dental plaque biofilm might be readily recognized by gingival fibroblasts through TLR9. Upon the activation, gingival fibroblasts may release Ctsk, resulting in gingival degradation leading to the periodontal pocket formation. ANOVA with Tukey's multiple-comparison test (**b**). Data are presented as mean values ± SD; *$p < 0.05$.

Supplementary Files

This is a list of supplementary files associated with this preprint. Click to download.

- Kondoetal.SupplementaryInformationCommunBiol.pdf